ibid., **14**, 4381 (1986); chromosome 17q, probe THH 59: Y. Nakamura *et al., ibid.* **16**, 3598 (1988); chromosome 18p (27 informative tumors), probe B74: F. Morle *et al., Cytogenet. Cell Genet.* **37**, 544 (1984); chromosome 18q (53 informative tumors), probe OS-4: I. Nishisho *et al., Jpn. J. Hum. Genet.* **32**, 1 (1987); chromosome 18q, probe OLVII A8: O. Delattre *et al., Nucleic Acids Res.* **15**, 1343 (1987); chromosome 18q, probe HHH64: K. Yoshioka N. Yoshioka, K. Nakabepu, Y. Sakaki, *ibid.* **14**, 3147 (1986); chromosome 18q, probe ERT 25: U. Muller *et al., Cytogenet. Cell Genet.* **45**, 16 (1987); chromosome 19p (44 informative tumors), probe JCZ 3.1: Y. Nakamura *et al., Nucleic Acids Res.* **16**, 1229 (1988); chromsome 19q (37 informative tumors), probe RBI-4: C. Julier, E. Wolff, Y. Nakamura, R. White, *ibid.*, in press; chromosome 20p (46 informative tumors), probe CMM6: Y. Nakamura *et al.*, *ibid.* **16**, 5222 (1988); chromosome 20q (22 informative tumors), probe MS1-27: D. Barker, M. Schafer, R. White, *Cell* **36**, 131 (1984); chromosome 21q (27 informative tumors), probe MCT 15: Y. Nakamura *et al., Nucleic Acids Res.* **16**, 9882 (1988); chromosome 22q (41 informative tumors), probe EFZ 31: K. Krapcho *et al., ibid.*, p. 5221; chromosome 22q, probe A-EB2.3: C. M. Rubin *et al., ibid.*, p. 8741; chromosome 22q, probe EW7.2: T. Bragg, Y. Nakamura, E. Wolff, J.-M. Lalouel, R. White, *ibid.*, in press.

24. B. Vogelstein *et al., Cancer Res.* **47**, 4806 (1987).

25. We thank J. Wasmuth, S. Humphries, A. Jeffreys, J. P. Julien, M. Litt, J. L. Mandel, Y. Sakaki, S. Takai, J. Nishisho, U. Muller, G. Thomas, P. Lin, and C. Westbrook for providing probes and T. Gwiazda for preparation of the manuscript. Supported by the Clayton Fund, the McAshan Fund, the Howard Hughes Medical Institute, and training grants GM07309 and GM07184 and grants CA41183, CA47527, and CA35494 from the National Institutes of Health.

16 December 1988; accepted 7 February 1989

Regulation of Calcium Concentration in Voltage-Clamped Smooth Muscle Cells

PETER L. BECKER, JOSHUA J. SINGER, JOHN V. WALSH, JR., FREDRIC S. FAY

The regulation of intracellular calcium concentration in single smooth muscle cells was investigated by simultaneously monitoring electrical events at the surface membrane and calcium concentration in the cytosol. Cytosolic calcium concentration rose rapidly during an action potential or during a voltage-clamp pulse that elicited calcium current; a train of voltage-clamp pulses caused further increases in the calcium concentration up to a limit of approximately 1 μ*M*. The decline of the calcium concentration back to resting levels occurred at rates that varied with the calcium concentration in an apparently saturable manner. Moreover, the rate of decline at any given calcium concentration was enhanced after a higher, more prolonged increase of calcium. The process responsible for this enhancement persisted for many seconds after the calcium concentration returned to resting levels. Thus, the magnitude and duration of a calcium transient appear to regulate the subsequent calcium removal.

IN SMOOTH MUSCLE, AS IN SKELETAL and cardiac muscle, cytosolic calcium concentration ($[Ca^{2+}]$) is the principal regulator of contraction (*1*). In contrast to the two types of striated muscle (*2, 3*), however, the relation between membrane electrical events and the rise and fall of cytosolic $[Ca^{2+}]$ has not been examined directly in smooth muscle on the time scale of physiological events. We have measured $[Ca^{2+}]$ with high-time resolution in voltage-clamped single smooth muscle cells, thus allowing simultaneous monitoring of Ca^{2+} currents (I_{Ca}) and changes in cytosolic $[Ca^{2+}]$. Furthermore, because Ca^{2+} influx could be rapidly initiated and terminated by using the voltage-clamp technique, we could study the processes responsible for restoring cytosolic $[Ca^{2+}]$ to resting levels. These techniques have enabled us to describe several kinetic and regulatory characteristics of the processes that control the $[Ca^{2+}]$, and thus contraction, of smooth muscle.

We used single smooth muscle cells isolated from toad stomach (*4*) that were loaded with the fluorescent Ca^{2+} indicator fura-2 (*5, 6*). Cytoplasmic $[Ca^{2+}]$ was measured with a high-time resolution microfluorimeter (*7*). Membrane potential and ionic currents were monitored with a single microelectrode (*8*) rather than a patch electrode to avoid dialysis of the cytoplasm and thus minimize the loss of factors that might be important in buffering or regulating the $[Ca^{2+}]$. In 20 m*M* extracellular Ca^{2+}, the resting cytosolic $[Ca^{2+}]$ in relaxed, microelectrode-impaled smooth muscle cells averaged 226 ± 22 n*M* (mean ± SEM; n = 17), a value similar to that reported in unimpaled cells (*9*).

Transient elevations in the cytosolic $[Ca^{2+}]$ occurred in response to action potentials (APs) induced at the offset of a hyperpolarizing current or in response to depolarizing command pulses under voltage clamp (Fig. 1). The average increase in $[Ca^{2+}]$ in response to either type of stimulation was 379 ± 32 n*M* (n = 25). During an AP, in which inward current is carried exclusively by Ca^{2+} (*10*), the rise in $[Ca^{2+}]$ occurred most rapidly starting at a potential of about −20 mV, and this rapid phase ended after the AP reached its peak (Fig. 1, A and B). Typically, a slow, small rise occurs as the potential rises through the range of −35 to −20 mV. During a depolarizing voltage-clamp command pulse, the rise in $[Ca^{2+}]$ was roughly proportional to the cumulative inward I_{Ca} (Fig. 1D) for the initial 100 to 200 ms (*11*), a period when the magnitude of the inward I_{Ca} was large. This observation, coupled with the fact that the $[Ca^{2+}]$ continues to rise throughout the AP suggests that, unlike skeletal muscle, the rise in cytosolic $[Ca^{2+}]$ depends strongly on Ca^{2+} influx through voltage-dependent sarcolemmal Ca^{2+} channels. Toward the end of a 2-s command pulse, the I_{Ca} declined, and the $[Ca^{2+}]$ either rose slowly or started to fall. However, in all cases the $[Ca^{2+}]$ declined more rapidly upon repolarization, suggesting that Ca^{2+} influx persisted as long as the cell was depolarized.

Although the rise in $[Ca^{2+}]$ appeared roughly proportional to the integrated inward I_{Ca}, the amount of Ca^{2+} entry determined by integrating the I_{Ca} far exceeded that calculated from the measured free $[Ca^{2+}]$ change. For example, integration of the I_{Ca} during the first 50 ms of the command pulse in Fig. 1D indicated a Ca^{2+} entry sufficient to elevate the $[Ca^{2+}]$ by 19 μ*M*, 40-fold greater than the measured 0.47 μ*M* change in the free $[Ca^{2+}]$ (*12*). Thus, most of the Ca^{2+} that crosses the sarcolemma must be binding to Ca^{2+} buffers, a conclusion consistent with current estimates of the physiological Ca^{2+} buffering capacity in smooth muscle (*13*).

A train of depolarizing command pulses produced summation of the $[Ca^{2+}]$ (Fig. 2). However, each successive pulse resulted in a smaller increase in $[Ca^{2+}]$, and a steady-state ceiling was reached. This ceiling averaged 856 ± 57 n*M* (n = 20), similar to the value obtained in response to cholinergic agonists or high K^+ concentrations in non–voltage-clamped cells (*14*). Several factors appear to be responsible for this ceiling. Peak I_{Ca} decreased with successive voltage-clamp pulses (Fig. 2B), presumably because of the inactivation of Ca^{2+} channels (*15*). Furthermore, as discussed below, the processes responsible for lowering the $[Ca^{2+}]$ are accelerated after a higher intracellular $[Ca^{2+}]$ is achieved.

On termination of a depolarizing command pulse, the I_{Ca} was also terminated, and the processes responsible for Ca^{2+} removal from the cytosol could be studied in isolation. The relation between the rate of

Department of Physiology, University of Massachusetts Medical School, Worcester, MA 01655.

$[Ca^{2+}]$ decline ($d[Ca^{2+}]/dt$) and the cytoplasmic $[Ca^{2+}]$ is shown for a single transient in Fig. 3. Although the decline in the $[Ca^{2+}]$ was faster at higher $[Ca^{2+}]$'s, the underlying process appears to be saturable because the relation between $d[Ca^{2+}]/dt$ and $[Ca^{2+}]$ was less steep at higher $[Ca^{2+}]$'s. This is in contrast to the nonsaturable relation in skeletal muscle (*2*) and molluscan neurons (*16*). If we assume a constant Ca^{2+} buffering capacity over this concentration range, the extent of curvature in the relation between $d[Ca^{2+}]/dt$ and $[Ca^{2+}]$ in Fig. 3 is consistent with a process that has an apparent Michaelis constant (K_m) for Ca^{2+} in the range of several hundred nanomolar and that operates against a continual inward Ca^{2+} leak. Such a low K_m suggests that the decline in $[Ca^{2+}]$ over this concentration range is predominantly due to sarcolemmal or sarcoplasmic reticulum Ca-ATPase pumps (*17, 18*), rather than to the lower affinity Na-Ca exchange mechanism (*19*).

The rate of $[Ca^{2+}]$ decline at any given level of $[Ca^{2+}]$ was enhanced after higher, more prolonged increases in $[Ca^{2+}]$. This enhancement is illustrated in Fig. 4, A and B, which shows four $[Ca^{2+}]$ transients induced by different voltage-clamp protocols. The rate of $[Ca^{2+}]$ decline of transient 3, which achieved a higher peak $[Ca^{2+}]$, is greater than that of transient 1 at every $[Ca^{2+}]$. The magnitude of enhancement in transient 3 is typical of this phenomenon, which was observed in 24 of 25 cells examined. Moreover, the process responsible for the enhancement observed after prolonged stimulation persisted even after $[Ca^{2+}]$ had returned to basal levels, as seen in Fig. 4, A and B, by a comparison of the rate of $[Ca^{2+}]$ decline in transient 4 with that of transient 1. This enhancement process gradually diminished over a period of about 30 s (Fig. 4, C and D). A qualitative indication that this enhancement process persists after the $[Ca^{2+}]$ returns to rest is the presence of an "undershoot" in $[Ca^{2+}]$ after prolonged elevation (for example, transient 3 in Fig. 4A). Such "undershoots" lasted approximately as long as the enhancement process persisted. An "undershoot" in the $[Ca^{2+}]$, which was observed in 14 out of 16 cells, would be expected if an enhancement of Ca^{2+} removal persisted beyond the period of $[Ca^{2+}]$ elevation.

Although the precise mechanism of the enhancement of the decline in $[Ca^{2+}]$ is not

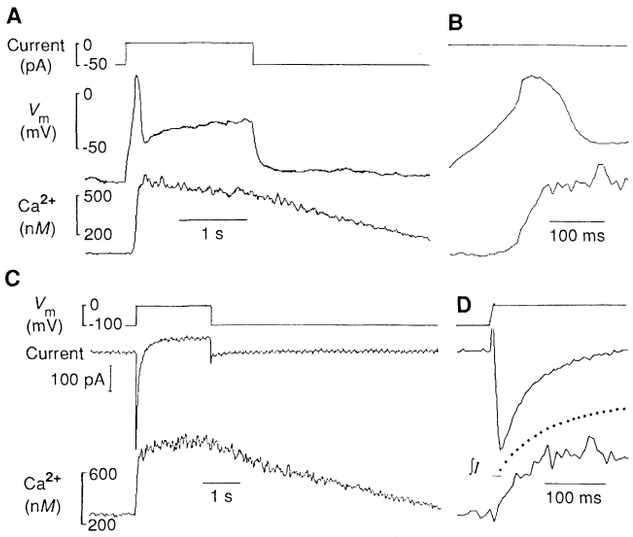

Fig. 1. Ca^{2+} transients and membrane potential (V_m) resulting from a single AP or a single depolarizing voltage-clamp pulse. (**A**) and (**B**) show low- and high-time resolution view, respectively, of the membrane potential and the $[Ca^{2+}]$ during an AP induced by the cessation of a hyperpolarizing current. (**C**) and (**D**) show low- and high-time resolution records, respectively, of membrane potential, membrane current, and the Ca^{2+} transient under voltage clamp during a 2-s depolarizing command pulse to 0 mV from a holding potential of −100 mV. In addition, (D) displays a plot of the integrated inward current during the initial period of the depolarizing command pulse. The current was integrated by measuring the area between the current trace and the current level at the end of the 2-s command pulse. The Ca^{2+} traces in (A) and (C) were smoothed by using an averaging interval of ~300 ms to reduce noise. The Ca^{2+} traces in (B) and (D) were not smoothed. $[Ca^{2+}]$ scales in this figure and Figs. 2 to 4 are linear. Capacitive transients are not apparent in (C) because not every sampled point was displayed. Bath solution contained 20 m*M* Ca^{2+} and 10 m*M* TEA. In (C) and (D), the microelectrode contained 3*M* CsCl. The larger fluctuations in the Ca^{2+} trace at higher $[Ca^{2+}]$s are not biological but reflect the fact that the raw 340- and 380-nm photon counts have a signal-dependent noise component that, because of the relation between $[Ca^{2+}]$ and the 340/380 fluorescence ratio, causes a higher absolute noise at higher $[Ca^{2+}]$'s. The dependence of the noise level on $[Ca^{2+}]$ is also observed in test solutions of fura-2 containing different $[Ca^{2+}]$'s.

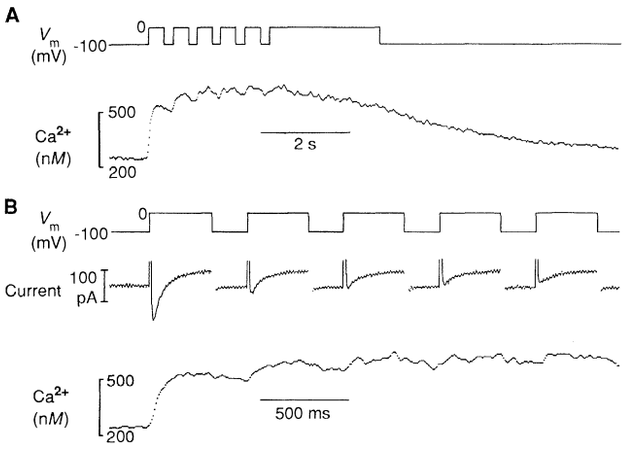

Fig. 2. Summation of the $[Ca^{2+}]$ during a train of voltage-clamp pulses. (**A**) The membrane potential and $[Ca^{2+}]$ during a train of five 300-ms command pulses to 0 mV from a holding potential of −100 mV, followed by a 2.5-s command pulse. (**B**) A higher time resolution view of the first five voltage-clamp pulses from (A) showing the membrane current in addition to the voltage and $[Ca^{2+}]$. The large current transients at the termination of the voltage-clamp pulse were blanked for a 20-ms period for clarity. Microelectrode contained 3*M* CsCl.

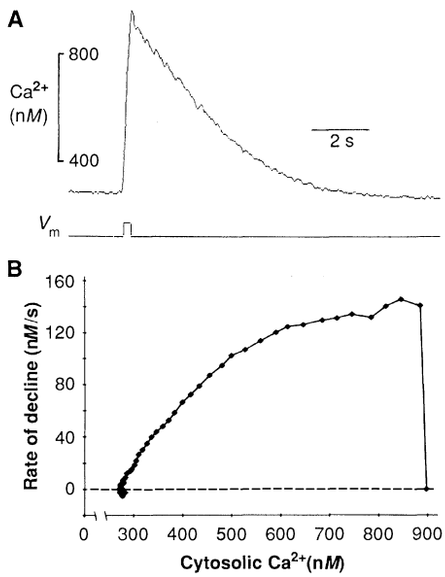

Fig. 3. (**A**) $[Ca^{2+}]$ as a function of time and (**B**) $d[Ca^{2+}]/dt$ as a function of $[Ca^{2+}]$ resulting from a single 300-ms depolarizing voltage-clamp command pulse to 0 mV from a holding potential of −100 mV. Ca^{2+} trace in (A) was smoothed with an averaging interval of approximately 50 ms. In (B), consecutive symbols represent estimates of $d[Ca^{2+}]/dt$ taken 250 ms apart. The rate of $[Ca^{2+}]$ decline plotted in (B) was estimated by the slope of a linear fit to the $[Ca^{2+}]$ data. We used a 0.5-s interval of the $[Ca^{2+}]$ data to determine the slope immediately after the clamp pulse, and this interval was extended to 2-s at later points to reduce noise. Thus, the $d[Ca^{2+}]/dt$ values calculated near the peak of the $[Ca^{2+}]$ are noisier and show more variation because of the smaller number of data points used to calculate $d[Ca^{2+}]/dt$. The $[Ca^{2+}]$ paired with each $d[Ca^{2+}]/dt$ measurement was taken as the average $[Ca^{2+}]$ over a 250-ms time interval.

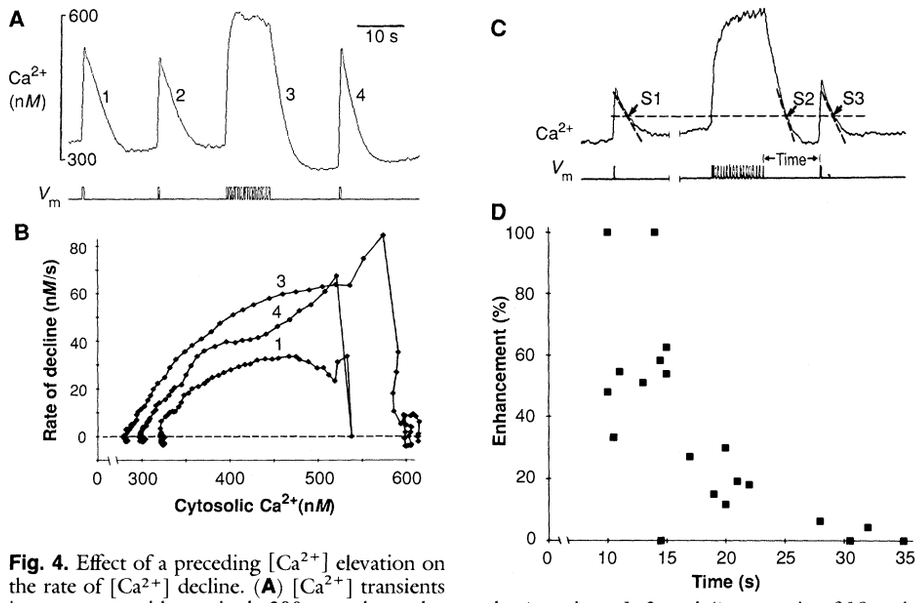

Fig. 4. Effect of a preceding $[Ca^{2+}]$ elevation on the rate of $[Ca^{2+}]$ decline. (**A**) $[Ca^{2+}]$ transients in response to either a single 300-ms voltage-clamp pulse (transients 1, 2, and 4) or a train of 19 such pulses (transient 3). Ca^{2+} trace in (A) was smoothed by using an averaging interval of ~300 ms. Greater $[Ca^{2+}]$ rise in transient 4 (compared with 1) was accompanied by proportionately more inward current (not shown). (**B**) The rate of $[Ca^{2+}]$ decline plotted as a function of $[Ca^{2+}]$ for transients 1, 3, and 4. For each trace, consecutive symbols are 250 ms apart. The upturn in $d[Ca^{2+}]/dt$ at the right of the numbers 3 and 4 in (B) was not a consistent observation. Increased variability in this region may be due to the smaller $[Ca^{2+}]$ data set used to determine $d[Ca^{2+}]/dt$ at the onset of the decay of the transient (see legend to Fig. 3). (**C**) Records illustrating the protocol for determining the time course of the persistence of the enhancement of Ca^{2+} removal as plotted in (D). A brief control elevation of the $[Ca^{2+}]$ was generated and then a prolonged elevation (>5 s); subsequently, brief test $[Ca^{2+}]$ elevations were generated at various intervals after the prolonged elevation. Then $d[Ca^{2+}]/dt$ was measured at an intermediate $[Ca^{2+}]$ during each transient (S1, S2, and S3). (**D**) The percentage of enhancement in each test $[Ca^{2+}]$ transient, calculated as $[(S3 - S1)/(S2 - S1)] \times 100$, plotted as a function of the time interval between the prolonged elevation and brief test pulse (data are from a total of seven cells).

clear, a number of possibilities can be excluded on the basis of available data. The enhancement was observed in unimpaled cells exposed to high K^+ concentrations. It did not correlate either with contraction or with changes in the membrane-holding current. These observations indicate that the mechanism is not based on either electrode impalement, cell shape change, or a change in the basal Ca^{2+} leak. We observed no evidence that the ability to elevate the $[Ca^{2+}]$ is impaired during the time that the enhancement persists, which indicates that the mechanism is not based on a depolarization-induced depletion of an internal Ca^{2+} store. It is more likely that enhancement of net Ca^{2+} removal results from a feedback stimulation by $[Ca^{2+}]$ on Ca^{2+} extrusion mechanisms. Sarcolemmal Ca^{2+} pumps in these and other smooth muscles are stimulated by a Ca^{2+}-calmodulin–dependent mechanism (*18, 20*), and in some smooth muscle cells sarcoplasmic reticulum Ca^{2+} pumps may be regulated by Ca^{2+}-calmodulin–dependent phosphorylation of the regulatory protein phospholamban (*21*). Thus, a prolonged rise in $[Ca^{2+}]$ could cause a persistent stimulation of membrane-associated Ca^{2+} pumps.

The enhancement of the $[Ca^{2+}]$ decline in smooth muscle is the opposite of what has been observed in skeletal muscle, in which prolonged $[Ca^{2+}]$ elevations induced a slowing of the rate of $[Ca^{2+}]$ decline (*2*). A more complicated response exists in molluscan neurons, where the initial rate of $[Ca^{2+}]$ decline after $[Ca^{2+}]$ elevations of longer duration was faster, although the later rate of decline was slower (*16*). The enhancement of the rate of $[Ca^{2+}]$ decline by a high $[Ca^{2+}]$ increase characterized in our study may be important for the normal function of gastric muscle, in which contraction must be phasic for the tissue to function properly. A persistent enhancement of Ca^{2+} removal induced by high $[Ca^{2+}]$ would tend to limit the duration of a contraction. Furthermore, such a process may also be a component underlying the sustained $[Ca^{2+}]$ oscillations observed in many cell types (*22*).

REFERENCES AND NOTES

1. A. P. Somlyo, *Circ. Res.* **57**, 497 (1985); K. E. Kamm and J. T. Stull, *Annu. Rev. Pharmacol. Toxicol.* **25**, 593 (1985).
2. J. R. Blinks, R. Rüdel, S. R. Taylor, *J. Physiol. (London)* **277**, 291 (1978); R. Miledi, I. Parker, P. H. Zhu, *ibid.* **333**, 655 (1982); W. Melzer, E. Rios, M. F. Schneider, *ibid.* **372**, 261 (1986).
3. C. C. Ashley and E. B. Ridgway, *ibid.* **209**, 105 (1970); L. Barcenas-Ruis and W. G. Wier, *Circ. Res.* **61**, 148 (1987); M. B. Cannell, J. R. Berlin, W. J. Lederer, *Science* **238**, 1419 (1987).
4. F. S. Fay, R. Hoffman, S. LeClair, P. Merriam, *Methods Enzymol.* **85**, 284 (1982).
5. Cells were loaded with fura-2 as described (*6*), producing an intracellular fura-2 concentration of approximately 30 μM. The cell chamber solution contained 94.0 m*M* NaCl, 3.0 m*M* KCl, 20.0 m*M* $CaCl_2$, 1.0 m*M* $MgCl_2$, 5.0 m*M* Hepes, and 10.0 m*M* tetraethylammonium (TEA), *p*H adjusted to 7.6 with NaOH. The high extracellular $[Ca^{2+}]$ is important for maintaining a high-resistance seal between the electrode and membrane (*10*). Solutions bathing the cells were continually exposed to 100% N_2 gas to minimize photobleaching of fura-2 [P. L. Becker and F. S. Fay, *Am. J. Physiol.* **253**, C613 (1987)]. Fura-2 and low O_2 concentrations did not appear to affect either action potentials or inward currents under voltage clamp, because both were qualitatively similar to those measured in non-loaded, normoxic cells (*10, 15*); see also (*6*).
6. S. Yagi, P. L. Becker, F. S. Fay, *Proc. Natl. Acad. Sci. U.S.A.* **85**, 4109 (1988).
7. The high-time resolution microfluorimeter has been described (*6*). Briefly, the excitation light is rapidly altered (~145 Hz) between 340 and 380 nm. Emission light is collected by a photomultiplier tube (PMT) operating in photon-counting mode. A mask at an intermediate image plane in the emission path limits the region of the field of view that is focused on the PMT. Generally, this mask was wider than a cell but about half of a cell length. Membrane potential and membrane current were sampled and stored twice per wavelength pair. The 340- and 380-nm fluorescence values were corrected for background fluorescence but not for cell autofluorescence, which was typically <2% of the signal observed in fura-2–loaded cells. The 340/380 fluorescence ratio was calculated by dividing a particular 340-nm photon count by the average of the two 380-nm photon counts that preceded and followed it. $[Ca^{2+}]$ was calculated by the ratio method [G. Grynkiewicz, M. Poenie, R. Y. Tsien, *J. Biol. Chem.* **260**, 3440 (1985)], using a dissociation constant of 200 n*M* (*9*). Maximum and minimum 340/380 fluorescence ratios determined in calibration solutions (*9*) were decreased by 15% to correct for possible intracellular viscosity effects on the dye [M. Poenie, J. Alderton, R. Steinhardt, R. Tsien, *Science* **233**, 886 (1986)].
8. Cells were impaled with borosilicate microelectrodes (20 to 60 megohm) filled with either 3*M* KCl (for action potential studies) or 3*M* CsCl (for voltage clamp), the latter to block K^+ currents. Membrane potentials were monitored with a microprobe system (World Precision Instruments, model M-707A). Voltage clamp was achieved with an external feedback circuit [S. M. Sims, J. J. Singer, J. V. Walsh, *J. Physiol. (London)* **367**, 503 (1985)]. The current output was filtered with a simple RC (resistor capacitor) circuit having a time constant of 5 ms (−3 dB at 31.8 Hz). Current and membrane potential were recorded directly on a chart recorder and sampled approximately every 3.5 ms by a computer.
9. D. A. Williams, K. E. Fogarty, R. Y. Tsien, F. S. Fay, *Nature* **318**, 558 (1985).
10. J. J. Singer and J. V. Walsh, *Am. J. Physiol.* **239**, C153 (1980); *ibid.*, p. C175; J. V. Walsh and J. J. Singer, *ibid.*, p. C162; *ibid.*, p. C182.
11. If the inward current was terminated after only 25 to 50 ms, the rise in $[Ca^{2+}]$ indicated by the fura-2 signal abruptly terminated, indicating that in these smooth muscle cells fura-2 can closely track the $[Ca^{2+}]$.
12. Our calculation assumed a 6-pl cell volume [C. R. Scheid and F. S. Fay, *Am. J. Physiol.* **246**, C422 (1984)] and no additional Ca^{2+} entry into the cytosol from any source. The contribution of fura-2 buffering is calculated to be approximately 6 μM over the indicated free $[Ca^{2+}]$ interval, given our estimated fura-2 concentration.
13. M. Bond, H. Shuman, A. P. Somlyo, A. V. Somlyo, *J. Physiol. (London)* **357**, 185 (1984).
14. D. A. Williams, P. L. Becker, F. S. Fay, *Science* **235**, 1644 (1987); this report also shows that the ceiling is not due to fura-2 saturation.
15. J. V. Walsh and J. J. Singer, *Pfluegers Arch.* **408**, 83 (1987).

16. Z. Ahmed and J. A. Connor, *Cell Calcium* **9**, 57 (1988).
17. A. K. Grover, C. Y. Kwan, P. J. Oakes, *Am. J. Physiol.* **248**, C449 (1985).
18. P. Lucchesi, R. A. Cooney, C. Mangsen-Baker, T. W. Honeyman, C. R. Scheid, *ibid.* **255**, C226 (1988).
19. M. A. Matlib, M. Kihara, C. Farrell, R. C. Dage, *Biochim. Biophys. Acta* **939**, 173 (1988); N. Morel and T. Gotfraind, *Biochem. J.* **218**, 421 (1984); R. S. Slaughter, A. F. Welton, D. W. Morgan, *Biochim. Biophys. Acta* **904**, 92 (1987).
20. F. Wuytack, G. De Schutter, R. Casteels, *Biochem. J.* **198**, 265 (1981); N. Morel, M. Wibo, T. Gotfraind, *Biochim. Biophys. Acta* **644**, 82 (1981).
21. L. Raeymaekers and L. R. Jones, *Biochim. Biophys. Acta* **882**, 258 (1986); J. A. Eggermont, M. Vrolix, L. Raeymaekers, F. Wuytack, R. Casteels, *Circ. Res.* **62**, 266 (1988).
22. N. M. Woods, K. S. R. Cuthbertson, P. H. Cobbold, *Nature* **319**, 600 (1986); R. Jacob, J. E. Merritt, T. J. Hallam, T. J. Rink, *ibid.* **335**, 40 (1988); M. J. Berridge and A. Galione, *FASEB J.* **2**, 3074 (1988).
23. We thank A. Gorzocoski, K. Fogarty, and S. Abramson for technical assistance. Supported by NIH grants (HL-14523, AM07807, and DK31620), NSF grant DCB8511674, and a grant from the Muscular Dystrophy Association.

23 November 1988; accepted 27 January 1989

Influence of the Major Histocompatability Complex on Positive Thymic Selection of $V_\beta17a^+$ T Cells

MARCIA A. BLACKMAN, PHILIPPA MARRACK, JOHN KAPPLER

A monoclonal antibody was used to show directly positive thymic selection of the T cell repertoire in mouse strains expressing the 17a β-chain variable domain ($V_\beta17a$) of the T cell receptor. In the absence of the potent tolerizing class II major histocompatability complex (MHC) molecule, I-E, peripheral expression of $V_\beta17a^+$ T cell receptors varied with the MHC haplotype of the mouse strain. In the most extreme case, H-2^q mice expressed high peripheral levels of $CD4^+$ $V_\beta17a^+$ T cells (14 to 19 percent), whereas H-2^b mice expressed low levels (3 to 4 percent). Analysis of (b × q)F_1 mice and chimeric mice showed that these differences were determined by positive thymic selection and implicated the thymic epithelium as the controlling cell type.

T CELL SPECIFICITY IS DIRECTED TOward antigen (Ag) that is complexed with a cell-surface molecule encoded by the MHC. Also, T cells preferentially recognize antigen in association with the organism's own MHC haplotype—a phenomenon termed self-MHC restriction—and yet cannot respond to self-MHC alone (self-tolerance). The T cell receptor (TCR) is a heterodimer, consisting of an α and a β chain. In addition to the TCR, which provides the specificity for Ag/MHC, T cells bear "accessory" molecules, CD4 and CD8, which bind monomorphic determinants on class II and class I MHC molecules, respectively. In the periphery, class I–restricted T cells are almost exclusively $CD8^+$, whereas class II–restricted cells are $CD4^+$. Thus, peripheral T cells are self-MHC–restricted, tolerant to self, and express an accessory molecule appropriate to the cell's MHC restriction. The process of T cell maturation in the thymus that produces such a precisely defined repertoire is believed to involve two selection events, a positive selection of T cells bearing TCRs biased toward self-MHC and a negative selection, or elimination, of T cells with autoreactive receptors.

Attempts to study thymic development have been hampered by the inability to measure populations of antigen-specific T cells directly. Recently, two new experimental approaches have been used: monoclonal antibodies (MAbs) that bind populations of TCRs that share some features of their structure and specificity (*1–3*) and TCR (αβ) transgenic mice that express predominantly one defined T cell specificity (*4–6*). We have examined the mechanism of tolerance to self-MHC with a MAb, KJ23a, that recognizes TCRs expressing the 17a β-chain variable region ($V_\beta17a$) (*1, 7, 8*). Because of the presence of a nonfunctional allele, $V_\beta17b$, in many strains of mice, $V_\beta17a$ has a restricted strain distribution (*9*). In $V_\beta17a^+$ strains of mice, TCRs that bear this V_β region react with high frequency to the class II MHC molecule, I-E. Antibody to $V_\beta17a$ could therefore be used to follow a population of T cells with a defined reactivity pattern. Mouse strains expressing I-E molecules had dramatically reduced peripheral expression of $V_\beta17a$ receptors. Examination of thymocytes in these I-E–tolerant mice showed that tolerance to self-MHC is mediated by clonal deletion of cells bearing autoreactive receptors during the immature, "double-positive" ($CD4^+/CD8^+$) stage of thymocyte maturation in the cortex (*1*). The presence of I-E on bone marrow–derived cells alone was sufficient to induce tolerance in the periphery (*7*).

Positive selection is less well characterized. The bias of the T cell repertoire to preferential recognition of antigen in the context of self-MHC is thought to reflect a positive selection event in the thymus, that is, only receptors capable of recognizing self-MHC (presumably in association with self-peptides) are given a signal to mature, but the evidence in support of positive selection has been indirect. Many (*10, 11*), but not all (*12*), studies in chimeric mice show that the peripheral repertoire is skewed toward recognition of antigen in the context of the MHC haplotype expressed in the thymus, and, in particular, the thymic epithelium [(*13*), but see (*14*)]. The interpretation of these studies has been made equivocal by the fact that the repertoire was measured by antigen reactivity (requiring immunization of experimentally manipulated animals), which might be influenced by peripheral and regulatory factors. Recently, positive selection was studied in TCR (αβ) transgenic mice (*5*). The receptor (as well as the accessory molecule) of the transgenic mice was preferentially expressed on T cells in mice of the MHC haplotype from which the receptor was originally cloned and not in two other haplotypes, implying positive selection by MHC in the absence of nominal antigen (*5*).

We report a direct demonstration of positive selection during thymocyte development, using the $V_\beta17a$ system previously used to define tolerance to self-MHC. An examination of peripheral $V_\beta17a$ TCR levels in mouse strains that do not express class II I-E molecules revealed a hierarchy of expression that correlated with MHC haplotype, such that H-2^q > H-2^s > H-2^b (Table 1A). Variation in expression was the greatest between H-2^q and H-2^b mice, particularly within the CD4 compartment of T cells (14 to 19% versus 3 to 4%). To confirm that the levels correlated with MHC haplotype and not strain-specific background genes, we bred the functional $V_\beta17a$ locus into B10 and B10.Q mice (*15*). The $V_\beta17a$ levels measured in these mice (Table 1A) confirmed the correlation with MHC haplotype.

The correlation between MHC and $V_\beta17a$ levels in the periphery is determined during thymic selection. We found that 10 to 11% of the immature cortical $\alpha\beta^+$ thymo-

M. A. Blackman, Howard Hughes Medical Institute at Denver, Department of Medicine, National Jewish Center for Immunology and Respiratory Medicine, Denver, CO 80206.
P. Marrack, Howard Hughes Medical Institute at Denver, Department of Medicine, National Jewish Center for Immunology and Respiratory Medicine, Denver, CO 80206, and Departments of Microbiology and Immunology, of Medicine, and of Biochemistry, Biophysics and Genetics, University of Colorado Health Sciences Center, Denver, CO 80262.
J. Kappler, Howard Hughes Medical Institute at Denver, Department of Medicine, National Jewish Center for Immunology and Respiratory Medicine, Denver, CO 80206, and Department of Microbiology and Immunology, University of Colorado Health Sciences Center, Denver, CO 80262.